

Spiral Weight for Modeling Cracks in Meshless Numerical Methods

Boris Muravin¹, Eli Turkel²

¹ Margan Physical Diagnostics Ltd., Ha-Omanut 12, Netanya, 42160, Israel
Tel: +972-9-8655510, Fax: +972-9-8655514, E-mail: bm@margan.com

² Department of Applied Mathematics, Tel-Aviv University, Tel-Aviv, Israel

Abstract

In the last decade several different approaches have been developed to study arbitrary static and dynamic cracks. Among these methods meshless techniques play an important role. These methods provide an accurate solution of a wide range of fracture mechanics problems while traditional methods such as finite element and boundary element have limitations. We wish to increase the accuracy of the meshless approximations without increasing the nodal density. This is done by an appropriate modification of the weight function near crack tips. Earlier attempts still had limitations that result in a lack of accuracy, especially in the case when a linear basis is used. In this work a new technique, *the spiral weight*, is introduced that minimizes the drawbacks of existing methods. Numerical examples show that the spiral weight method is more efficient than existing methods, when using a linear basis, for the solution of crack problems.

Keywords: Meshless methods, spiral weight, crack.

Introduction

The numerical solution by the traditional finite element method (FEM) of fracture mechanics problems with arbitrary dynamic cracks is limited to simple cases. This is because solution of growing discontinuities requires time consuming remeshing at every time step. For this reason adaptive FEM has become essential. However adaptive remeshing and mapping of variables is a difficult, computationally expensive task and is a source of cumulative numerical errors. The development of meshless methods [1-9] and the extended finite elements method (X-FEM) [10] in recent years have enabled the solution of growing cracks without remeshing. Nevertheless, these methods continue to be computationally expensive because of the large nodal densities in meshless methods and the fine meshes needed in X-FEM for an accurate solution. Therefore there is a constant effort to improve the accuracy without increasing the degrees of freedom.

We focus on improvements to meshless methods for the solution of fracture mechanics problems. Although X-FEM has recently received greater attention than meshless methods, they remain an efficient and accurate approach to solve fracture mechanics problems. Recent developments of meshless methods for the solution of different classes of problems such as multiple interacting cracks [11], 3D cracks [12], and cracks in elastic-plastic materials [13] improve these numerical methods to a new level, making them more attractive to the user.

There are two main approaches, in meshless methods, for modeling discontinuities and capturing singular stresses at the crack tip. The first one is based on incorporation of a jump function along the discontinuity and a specific near crack-tip displacement solution in the extrinsic basis [14]. This approach was adopted from X-FEM and has similar limitations. The enrichment area is limited when multiple cracks are densely distributed or when crack tips are close to the boundaries. Modeling of moving cracks in dynamic problems requires the incorporation of different near crack-tip solutions which depends on the crack velocity. In addition, enrichment for developing cracks in elastic-plastic materials is not yet established.

Many of these limitations can be avoided when using another approach which is based on a special modification of the weight functions at the crack tip. For this purpose, several methods have been devised: *the visibility* method [1,15], *the "see-through"* method [16], *the transparency* method [6,17], *the wedge model* [18] and *the diffraction* method [6,17]. The first developed schemes were the *visibility* and *"see-through"* methods. They provide an accurate solution only when very large nodal densities are used. In the visibility method, this is because the weight and shape functions are discontinuous near the crack tip and the size of the discontinuity is a function of the nodal spacing. Although, the "see-through" method provides continuous approximations, it effectively shortens the crack and does not properly capture the singular stress at the crack tip. The transparency method and the wedge model provide more accurate results, however they have a restriction on the position of nodes limiting their use in dynamic crack problems.

Most recently, Duflot and Nguyen-Dang [19] proposed an *enriched weight function* method. In this method the diffraction weight functions of three nodes near the crack tip are multiplied by the square root of the distance from the crack tip leading to more accurately capture of the singular stresses. However, no analysis of the displacement and the stress field at the crack tip was performed to demonstrate that only three enriched nodes are sufficient to capture the singular stresses and to enforce the zero displacement condition at the crack tip. Nevertheless, calculated stress intensity factors showed greater accuracy using the enriched weight functions compared with an ordinary diffraction approximation. In the current formulation, the enriched nodes are moved together with the crack tip. Hence, the application of this method appears to be limited to static and quasi static cases.

We consider below, in detail, the diffraction method, which has been shown to be an accurate method and is widely used for the solution of fracture mechanics problems. We modify this method taking into consideration the drawbacks of the methods described above to achieve a more accurate solution of arbitrary crack problems.

Diffraction method

The diffraction method [6,17] has been used extensively within the meshless methods and achieves accurate results. Furthermore, it possesses simplicity, a small dependence on the nodal distribution near the crack tip and produces continuous approximations. The method is called diffraction since the weight function encloses the crack surface similar to the way light diffracts around corners. In this method the

distance d_I between the node point x_I and sampling point x is modified for all points x for which the line (x_I, x) intersects the crack line, see Figure 1.

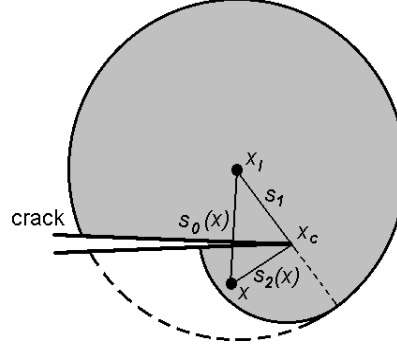


Figure 1. The weight functions by the diffraction method for single-crack problem.

The modified weight function distance d_I is given by:

$$d_I = \left(\frac{s_1 + s_2(x)}{s_0(x)} \right)^\lambda \cdot s_0(x), \quad (1)$$

where $s_1 = |x_I - x_c|$, $s_2(x) = |x - x_c|$, $s_0(x) = |x - x_I|$, x_I is the node, x is the sampling point, x_c is the coordinate of the crack tip, and λ is the diffraction method parameter. For problems with a normal nodal distributions and a linear basis, the parameter λ is chosen as 2. For the problems with enrichments, λ is equal either to 1 or 2.

The spatial derivatives of the weight function with the diffraction method are calculated by the chain rule:

$$\frac{dw}{dx_i} = \frac{\partial w}{\partial d_I} \frac{\partial d_I}{\partial x_i}, \quad (2)$$

$$\frac{\partial d_I}{\partial x_i} = \lambda \left(\frac{s_1 + s_2}{s_0} \right)^{\lambda-1} \frac{\partial s_2}{\partial x_i} + (1 - \lambda) \left(\frac{s_1 + s_2}{s_0} \right)^\lambda \frac{\partial s_0}{\partial x_i}, \quad (3)$$

where

$$\frac{\partial s_0}{\partial x_i} = \frac{x_i - x_{Ii}}{s_0}, \quad (4)$$

and

$$\frac{\partial s_2}{\partial x_i} = \frac{x_i - x_{ci}}{s_0}. \quad (5)$$

Spiral weight

To increase the accuracy of the approximation near cracks and their tips, we construct a new *the spiral weight* method. This takes into consideration the advantages and drawbacks of the diffraction method. The following are the main disadvantages of the diffraction method:

- The method does not properly capture the stress singularity at the crack tip when a linear basis is used. It does not preserve the discontinuity along the entire length of the crack. The maximum stress moves a small distance behind the crack tip. This leads to an effective shortening of the crack line.
- Solution enrichment, using a star-shaped array of nodes or else a significant mesh refinement is required to obtain an accurate solution. For problems where these techniques cannot be used, the accuracy of the method is not sufficient. This class of problems includes dynamic cracks, systems of strongly interacting cracks when the distances between the cracks tips are small and areas where the local enrichment covers a significant portion of the domain. In these cases the use of the fully enriched basis is complicated and computationally expensive. Difficulties also occur when the crack tips are close to the boundaries.

For a wide range of fracture mechanics problems the use of enrichment techniques is difficult or impossible. Therefore, it is important to develop a method which can accurately solve for the stresses even when using a linear basis. We shall try to achieve this goal with the spiral weight method.

In this method, the distance d_I between node x_I and sampling point x is modified when the line segment (x, x_I) crosses the crack. The modification is done according to the following rule:

$$d_I = d_I^d R_p + (1 - R_p) d_{ml}, \quad (6)$$

d_I^d is an initially modified distance between the point x and node x_I . d_{ml} is the size of the nodal domain of influence. R_p is an angular ramp function, to be presented.

The initially modified distance d_I^d can be calculated by either the diffraction or the transparency method. However, computations show that the diffraction method with $\lambda = 2$ applied for the calculation of d_I^d provides the most accurate results.

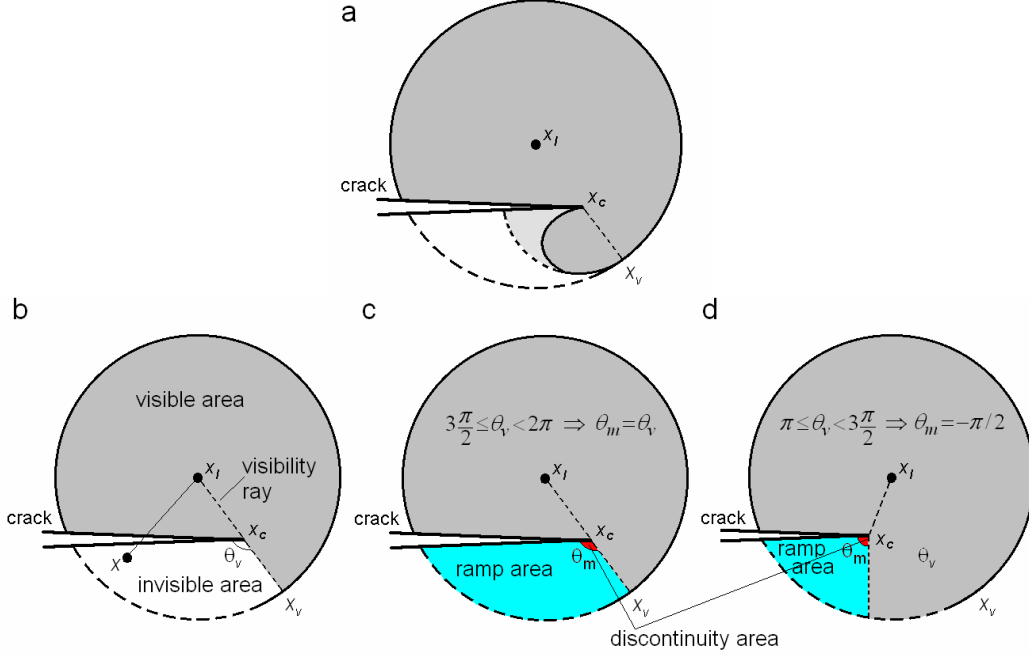


Figure 2. (a) The weight functions by the spiral method for single-crack problem. (b), (c), (d) definition of the spiral weight parameters.

In the following, we consider the construction of the angular ramp function R_p . We make the following definitions:

1. A point x is *invisible*, if it belongs to the nodal domain of influence of node x_I and line segment (x, x_I) crosses the crack (Figure 2b). The domain of all invisible points is the *invisible area* (Figure 2b).
2. The area around the crack tip x_c is divided into four quarters Q_i for $i=1..4$:

$$Q_i : \left((i-1)\frac{\pi}{2} \leq \theta < i\frac{\pi}{2} \right), \quad (7)$$

where θ is the angle with the crack line.

3. The *visibility ray* is the ray from node x_I passing through the crack tip x_c (Figure 2b).
4. Let x_v be a point that belongs to the visibility ray and is located at a distance d_{mI} from the crack tip. The *visibility angle* θ_v is the angle between the visibility ray and the crack line (Figure 2b).
5. The angle θ_m is given by:

$$\theta_m = \begin{cases} \pi/2, & \theta_v \in Q_1 \\ -\pi/2, & \theta_v \in Q_3 \\ \theta_v, & \text{otherwise} \end{cases}, \quad (8)$$

see (Figure 2c,d).

6. The *ramp area* is the part of the invisible area between the ray at angle θ_m and the crack line (Figure 2c,d).
7. The *discontinuity area* is the part of the ramp area which is located within a radius r_c from the crack tip (Figure 2c,d).

The angular ramp function $R_p(\theta)$ is constructed so that it satisfies the following conditions:

1. The function $R_p(\theta)$ is smooth and monotonically decreasing from 1 to 0.
2. At angle θ_m , $R_p(\theta_m)=1$.
3. At the crack surfaces: $R_p(\pm\pi)=0$.

The ramp functions suggested here, which satisfies above conditions is:

$$R_p(\bar{\theta}) = c \cdot \sin^n \bar{\theta}, \quad (9)$$

where $n=2 \cdot k+1$, $k=0 \dots 4$,

$$c = \begin{cases} 1, & \theta \in Q_{1,2} \\ -1, & \theta \in Q_{3,4} \end{cases}, \quad (10)$$

$$\bar{\theta} = \frac{(\theta - \theta_a)(\theta_d - \theta_c)}{\theta_b - \theta_a} + \theta_c, \quad (11)$$

where $\theta_a = \theta_m$, $\theta_b = \pi$, $\theta_c = \pi/2$, $\theta_d = \pi$ if $c=1$ and $\theta_a = -\pi$, $\theta_b = \theta_m$, $\theta_c = -\pi$, $\theta_d = -\pi/2$ if $c=-1$.

The derivatives of the ramp function (9) are:

$$R_{p,i}(\bar{\theta}) = c \cdot n \cdot \sin^{n-1} \bar{\theta} \cdot \cos \bar{\theta} \cdot \bar{\theta}_i, \quad (12)$$

where $i=x,y$ and

$$\bar{\theta}_{,x} = -\frac{\sin \theta}{r} \cdot \frac{\theta_d - \theta_c}{\theta_b - \theta_a}, \quad (13)$$

$$\bar{\theta}_{,y} = \frac{\cos \theta}{r} \cdot \frac{\theta_d - \theta_c}{\theta_b - \theta_a}, \quad (14)$$

r is the radial distance from point x to the crack tip.

Outside of the *ramp area* we set $R_p(\theta)=1$, $R_{p,i}=0$. The resulting ramp function and its x derivative around the crack tip are presented in Figure 3.

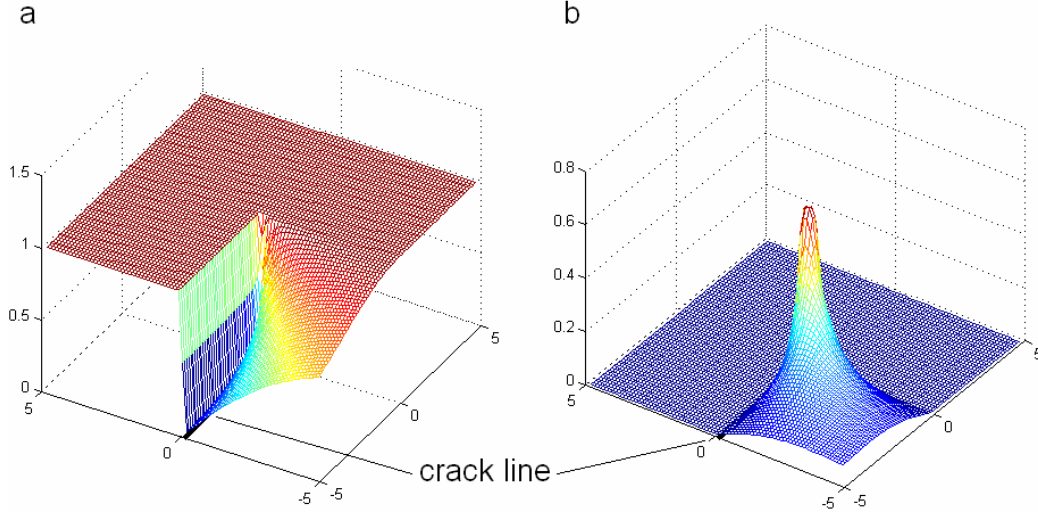


Figure 3. (a) The angular ramp function, (b) its x derivative. The crack line extends to the origin point $(0,0)$.

It should be noted that the ramp function and its derivatives are discontinuous at the crack tip. However, this should pose no difficulties since no quadrature points are placed at the crack tip.

For nodes that are located ahead of the crack tip, the *visibility angle* and consequently θ_m are smaller than 90 degrees. For small *visibility angles* the ramp function has a large gradient. The power n , in (9) is used as a parameter to adjust the rate of the ramp function changes in accordance with size of θ_m . We recommend setting $n=1$ for $\theta_m = \pm\pi/2$. For other angles θ_m smaller than 90 degrees, a larger n is advisable. The power $n=5$ is found to work well for such angles.

In the *discontinuity area*, the derivatives of the ramp function have a sharp gradient, which leads to a large gradient of the weight and shape function derivatives. This results in a lack of accuracy over the entire domain, and becomes a significant source of error. To minimize this effect, one of the following techniques can be used:

1. The ramp function and its derivatives are set equal to zero for all points that lie in the *discontinuity area*. Therefore, the area where the ramp function and its derivatives are discontinuous or have a sharp gradient is removed from the *ramp area*.
2. Alternatively, the ramp function is set equal to one and its derivatives equal to zero for all points that lie in the *discontinuity area*. Thus, the weight functions and their derivatives are calculated by the diffraction method in this small area.
3. A third technique is that the ramp function is not modified and the ramp function derivatives are set equal to certain constants in the *discontinuity area*.

$$R_{p,x} = c_1, \quad (15)$$

$$R_{p,y} = c \cdot c_2, \quad (16)$$

where c is defined in (10), and $c_{1,2}$ are constants.

The spiral weight method with all three techniques showed numerical convergence despite the discontinuities in the approximations. This is due to the local character of these discontinuities. It is established computationally that the discontinuity area with $r_c=0.1 d_{ml}$ provides the most accurate results. In this way, the *discontinuity area* vanishes as the number of nodes at the crack tip increases, especially when a star-shaped array of nodes is used. The third technique with constants $c_1=0.6$ and $c_2=1.4$ showed more accurate results than the two others. But for all three techniques, the results are more accurate than those from the diffraction method when using a linear basis.

Figure 4 presents the weight and shape functions and their x derivatives calculated by the spiral weight method. The nodal distribution is equally spaced with additional nodes around the crack line and at the crack tip. A linear basis is used for the shape function and its x derivative calculations.

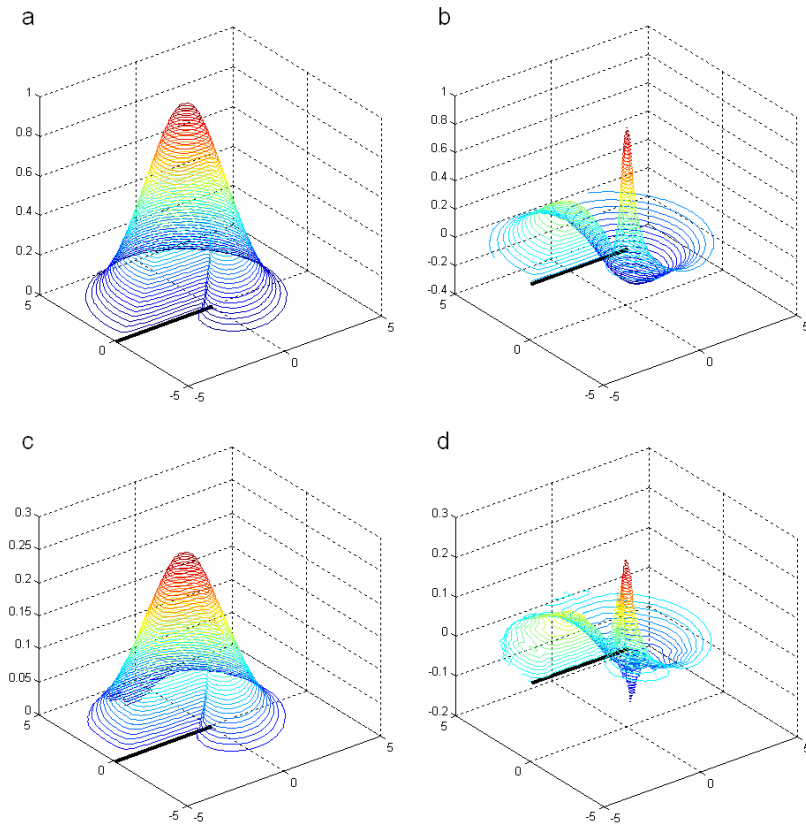


Figure 4. (a) Spline weight function, (b) its x spatial derivative, (c) shape function, (d) its x derivative by the spiral method near the crack tip.

In Figure 5 contour plots of weight functions calculated by the diffraction method and the spiral weight method are compared. One can see that the weight functions calculated by the spiral weight method (Figure 5b,d) preserve the discontinuity along the crack line while those calculated by the diffraction method do not (Figure 5a,c).

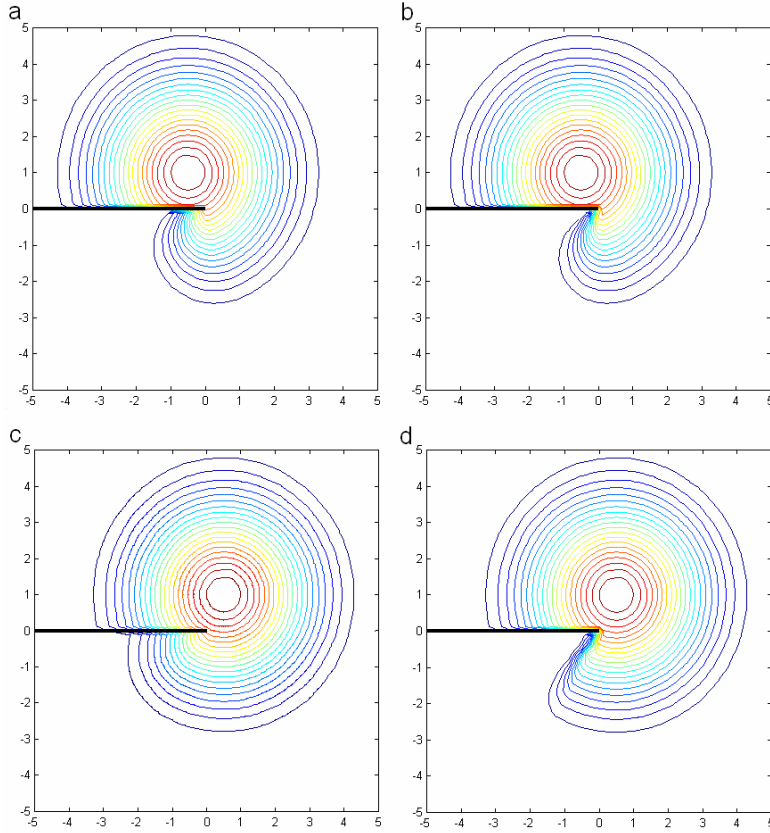


Figure 5. Comparison of weight function contours constructed by:
a. The diffraction method for node $x_f=(-0.5,1)$.
b. The spiral weight method for node $x_f=(-0.5,1)$.
c. The diffraction method for node $x_f=(0.5,1)$.
d. The spiral weight method for node $x_f=(0.5,1)$.

Numerical Example and Discussion

We now discuss the accuracy of the *spiral weight* method for the construction of weight functions near the crack tip compared with the diffraction method. We select a numerical example that has an analytical solution [20, 21] given in (17)-(18). The numerical example allows us to investigate the accuracy of the stress and displacement fields over the entire domain of the problem.

Mode I stress field:

$$\begin{aligned}
\sigma_{xx} &= \frac{K_I}{\sqrt{2\pi r}} \cos\left(\frac{\theta}{2}\right) \left[1 - \sin\left(\frac{\theta}{2}\right) \sin\left(\frac{3\theta}{2}\right) \right] \\
\sigma_{yy} &= \frac{K_I}{\sqrt{2\pi r}} \cos\left(\frac{\theta}{2}\right) \left[1 + \sin\left(\frac{\theta}{2}\right) \sin\left(\frac{3\theta}{2}\right) \right] \\
\tau_{xy} &= \frac{K_I}{\sqrt{2\pi r}} \cos\left(\frac{\theta}{2}\right) \sin\left(\frac{\theta}{2}\right) \cos\left(\frac{3\theta}{2}\right)
\end{aligned} \tag{17}$$

where K_I is the stress intensity factor, r and θ are polar coordinates with an origin at the crack tip σ_{ij} are components of the stress tensor, $i, j = x, y$.

Mode I displacement field:

$$\begin{aligned} u_x &= \frac{K_I}{2\mu} \sqrt{\frac{r}{2\pi}} \cos\left(\frac{\theta}{2}\right) \left[k - 1 + 2 \sin^2\left(\frac{\theta}{2}\right) \right] \\ u_y &= \frac{K_I}{2\mu} \sqrt{\frac{r}{2\pi}} \sin\left(\frac{\theta}{2}\right) \left[k + 1 - 2 \cos^2\left(\frac{\theta}{2}\right) \right] \end{aligned} \quad (18)$$

where u_i are components of the displacement, $i, j = x, y$, $k = 3 - 4\nu$ for plane strain, and $k = (3 - \nu)/(1 + \nu)$ for plane stress, ν is the Poisson ratio.

The numerical example is solved using the Element Free Galerkin (EFG) meshless numerical method [1-9]. In this example, an edge crack with length $a=5$ units in a square specimen with width and height of 10 units is investigated. The linear-elastic displacement field corresponding to mode I loading with $K_I=1$ is applied on the boundaries of the specimen. Plane stress conditions are assumed. The elastic modulus E is $30 \cdot 10^6$ and the Poisson's ratio, ν is 0.3. A Gauss quadrature rule with 8x8 Gauss points is used for the numerical integration, which is expressed for a two-dimensional function $f(x, y)$ over domain Ω as:

$$\int_{\Omega} f(x, y) d\Omega = \sum_{k=1}^n f(x_k, y_k) w_k, \quad (19)$$

(x_k, y_k) are the coordinates of a Gauss quadrature point; w_k is the weight of the Gauss quadrature point. n_q is the order of the Gauss quadrature rule.

The quadratic spline weight function (20) for a circular domain is applied:

$$w(d_I) = \begin{cases} 1 - 6 \cdot \left(\frac{d_I}{d_{ml}}\right)^2 + 8 \cdot \left(\frac{d_I}{d_{ml}}\right)^3 - 3 \cdot \left(\frac{d_I}{d_{ml}}\right)^4 & d_I \leq d_{ml} \\ 0 & d_I > d_{ml} \end{cases}, \quad (20)$$

where $d_I = \|x - x_I\|$ is the distance between point x and node x_I , d_{ml} is the domain of influence of node x_I , where

$$d_{ml} = d_{max} c_I, \quad (21)$$

where d_{max} and c_I are constants. c_I is the nodal spacing, which is the distance to the second nearest node for equally spaced nodes and the distance to the third nearest node for other nodal distributions. The value $d_{max}=2.5$ is used in all calculations. The Lagrange multiplier method [22] is applied to enforce the essential boundary conditions. A regular (equally spaced) nodal distribution is selected. Schemes 2 and 4 use additional star-shaped nodes that are added around the crack [16]. These nodes consist of three equally spaced rings of nodes. The radius of the external ring is equal

to 0.75 of the distance between regular nodes. The regular nodes that lie within the external ring of the star-shaped area are removed. Nodes of the star-shaped array that lie on the crack line are divided in two and moved to opposite sides of the crack. One more node is added at the crack tip in addition to the star-shaped array of nodes. In schemes 3-5, (see Table 1) the solution enrichment at the crack tip is implemented by a full basis enrichment technique [23].

Table 1. Distinctive ingredients of the numerical schemes.

Scheme number	Distinctive ingredients of the scheme *
1	Linear basis over the entire domain
2	Linear basis over the entire domain and star-shaped array of nodes local refinement
3	Local enrichment by fully enriched basis
4	Local enrichment by fully enriched basis and star-shaped array of nodes local refinement
5	Enrichment over the entire domain by fully enriched basis

* Common ingredients of the applied schemes are specified in the description of the numerical example.

To assess the accuracy of the solution, the energy (22) and L_2 norms of the numerical errors (24) are calculated. The energy norm of the error is computed by:

$$\varepsilon_{ij} = \frac{1}{2}(u_{j,i} + u_{i,j}), \quad (22)$$

where ε is the strain defined in (23).

The strain components for small displacements are:

$$\varepsilon_{ij} = \frac{1}{2}(u_{j,i} + u_{i,j}), \quad (23)$$

where index i after the comma represents differentiation in the direction of x if $i=1$, or y if $i=2$.

The L_2 norm is calculated by:

$$L_2 = \left[\int_{\Omega} (u^{approx} - u^{exact})^T (u^{approx} - u^{exact}) d\Omega \right]^{1/2}. \quad (24)$$

The numerical solution is compared with the analytical solution given in (17)-(18). The energy norm (22) and L_2 norm (24) of numerical errors as functions of the average nodal spacing, h are calculated and analyzed for different EFG schemes. The accuracy of the new technique, the spiral weight, is compared with the diffraction method. The effects of the full basis enrichment and star-shaped array of nodes refinement on the solution accuracy and its convergence are also investigated.

The results shown in Figure 6 demonstrate that the spiral weight method is more accurate than the diffraction method, especially when the EFG approximations are constructed with a linear basis. One of the reasons is that the weight functions, in the diffraction method, do not preserve the discontinuity along the crack line, as seen in Figures 5a,c. This leads to an effective shortening of the crack. In Figure 7a we see that the maximum stress moves a small distance behind the crack tip. Moreover the zero displacement condition at the crack tip is not satisfied. This effect can be reduced with higher nodal densities or nodal refinement at the crack tip. On the other hand, the spiral weight method is constructed to preserve the discontinuity along the entire length of the crack as is demonstrated by the results in Figures 5b,d. Figure 7b shows that the effect of the maximum stress moving behind the crack tip is minimized and the displacements vanish at the crack tip even without special nodal refinement.

In Figure 6 we show that the application of a star-shaped array of nodes for refinement at the crack tip improves the accuracy of the solution whether calculated by either the diffraction or the spiral method. Although the improvement is significant when using the diffraction method, the spiral method provides even more accurate results. In Figure 6b we see that the accuracy of the displacements, when calculated by the spiral method with a linear basis (scheme 1, see Table 1), is even greater than when calculated by the diffraction method with a linear basis and star-shaped nodes (scheme 2, see Table 1). The convergence rates when using either a linear basis or else when using a linear basis together with a star-shaped array of nodes refinement have similar values. The convergence rates for the spiral and the diffraction methods are found to be nearly identical in all cases. The convergence rate for schemes 1 and 2 is approximately 0.5 in the energy norm and 1.15 in the L_2 norm.

The full basis enrichment techniques should be applied only in the stress singularity dominated zone. In [24] Fleming suggests that one should set the radius of the enrichment zone to 10% of the crack length. The results in Figure 6 show that the full basis enrichment technique improves the accuracy of the solution calculated by both the diffraction and the spiral methods when a linear basis is used. The slope of the $\ln(\text{error})$ vs. $\ln(h)$ curve for this EFG scheme (scheme 3, see Table 1) is higher than for the linear basis and equals 1.12 for the energy norm and 2.15 for the L_2 norm. The accuracy is even greater when local enrichment is used and the star-shaped array of nodes is applied for local refinement at the crack tip as seen in Figures 6, 7c. This makes the full basis enrichment an effective tool for improving the solution. For this scheme (scheme 4, see Table 1) the convergence rate of the energy norm is 0.73 and 1.55 for the L_2 norm. For scheme 4, where the full basis enrichment and star-shaped array of nodes for nodal refinement are used, the accuracy of the spiral method and the diffraction method is almost identical.

We note that for sufficiently fine meshes, when the average distance between regular nodes h converges to zero, that both schemes 3 and 4 should provide similar results including the convergence rate. However, for the nodal densities we have considered the slope of scheme 3 is greater than for scheme 4, though scheme 4 is more accurate. This fact can be explained by the character of the coupling procedure of a locally enriched basis with a linear basis. Fine meshes result in a smoother transition from an enriched area to a linear area. For coarse meshes this coupling is one of the most significant sources of error. However, the error due to the coupling rapidly decreases

when we introduce a local refinement at the crack tip. This result in the greater slope for scheme 3 compared with scheme 4 for the considered nodal densities. For sufficiently fine meshes scheme 3 has the same convergence rate as scheme 4.

In the numerical example the analytical solution (17)-(18) is not limited to the area near the crack tip. Hence, we can apply the enriched basis *over the entire domain* of the problem (scheme 5, see Table 1). The results presented in Figures 6, 7d, and 8 show good agreement between the numerical solution and the analytical solution. We note that the calculated displacements match very well with the exact displacements. This indicates a proper enforcement of the essential boundary conditions by the Lagrange multiplier method. The convergence rate of this scheme is 0.50 for the energy norm and 1.07 for the L_2 norm. The accuracy of the solution by the diffraction and spiral weight methods are nearly identical, especially for the displacements as seen in Figure 6.

The errors in the energy calculated by the spiral weight method are slightly larger than by the diffraction method. This is due to local discontinuities of the spiral shape functions at the crack tip. Local discontinuities contribute a more significant portion of the total numerical error when solving the numerical example using scheme 5 compared with other schemes. Theoretically, for the approximations with fully enriched basis functions, there should be no errors due to approximations, since the basis functions include all the elements of the analytical solution. Other factors affecting the total accuracy of the solution include the numerical integration and the stiffness matrix inversion. However, use of the full basis enriched *over the entire domain* (scheme 5) is inappropriate for the solution of fracture mechanics problems except for this example.

The stress intensity factors are calculated to illustrate the improvement of the EFG method as a function of the number of nodes. The results are shown in Figure 9. Stress intensity factors calculated by the spiral weight method are more accurate than those obtained by the diffraction method with a linear basis. The errors in the stress intensity factors are 4 to 5 times lower compared with the diffraction method.

The accuracy of the stress intensity factor calculated by the spiral method using a linear basis is more than 99.4% for the coarsest mesh and 99.8% for the finest mesh. For the case of a locally enriched basis and local refinement at the crack tip the accuracy of both methods is nearly identical. For the coarsest mesh the accuracy is 99.8% and for the finest mesh it is 99.998%. When the fully enriched basis is applied over the entire domain the solutions provided by the diffraction and the spiral methods are nearly identical. For the finest nodal distribution the accuracy is 99.97% and for the finest mesh, it is 99.998%.

Based on the results for the tested schemes we conclude that:

1. The spiral weight method shows the same convergence rates as the diffraction method for all tested schemes.
2. For the schemes with a local enrichment one can use either the spiral or the diffraction method to obtain the same level of accuracy and efficiency. Both methods require similar computational times.

3. The most reliable, efficient and accurate EFG scheme should use a full basis enrichment in the vicinity of the crack tip and a star-shaped array of nodes and the diffraction or else the spiral weight methods for the construction of the weight functions near the crack tip (scheme 4).
4. The spiral weight method is more accurate than the diffraction method for the practically important case of a linear basis. The diffraction method, applied with a linear basis, has several disadvantages:
 - Incorrect capturing of the stress singularity at the crack tip.
 - The discontinuity along the entire length of the crack is not preserved.
 - Displacement of the maximum stress in a small distance behind the crack tip. This effectively shortens the crack line.

These disadvantages are minimized with the spiral weight method.

Therefore, for problems where the star-shaped arrays of nodes and full basis enrichment cannot be used, the spiral method is recommended (scheme 1 with the spiral weight method). This class of problems includes moving cracks and systems of strongly interacting cracks when the distances between the cracks tips are small, or areas of local enrichment cover a significant part of the domain and the use of the fully enriched basis is both complicated and computationally expensive, or when the crack tips are close to specimen boundaries

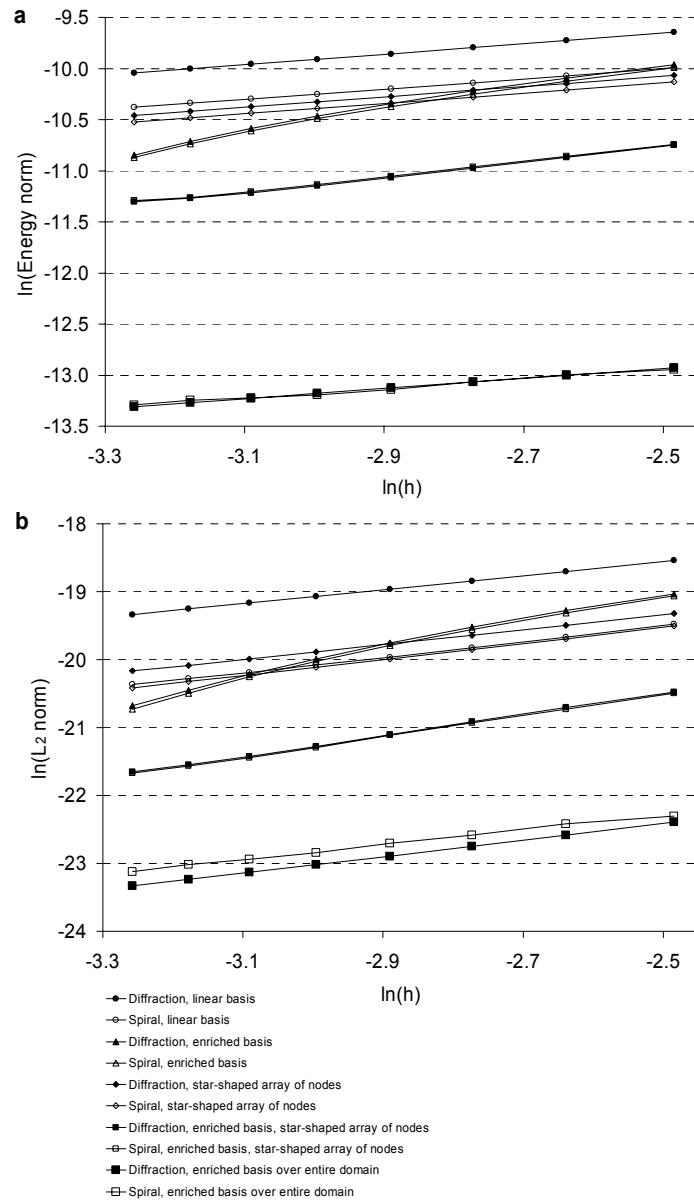


Figure 6. (a) The energy error norm, (b) the L2 error norm convergence.

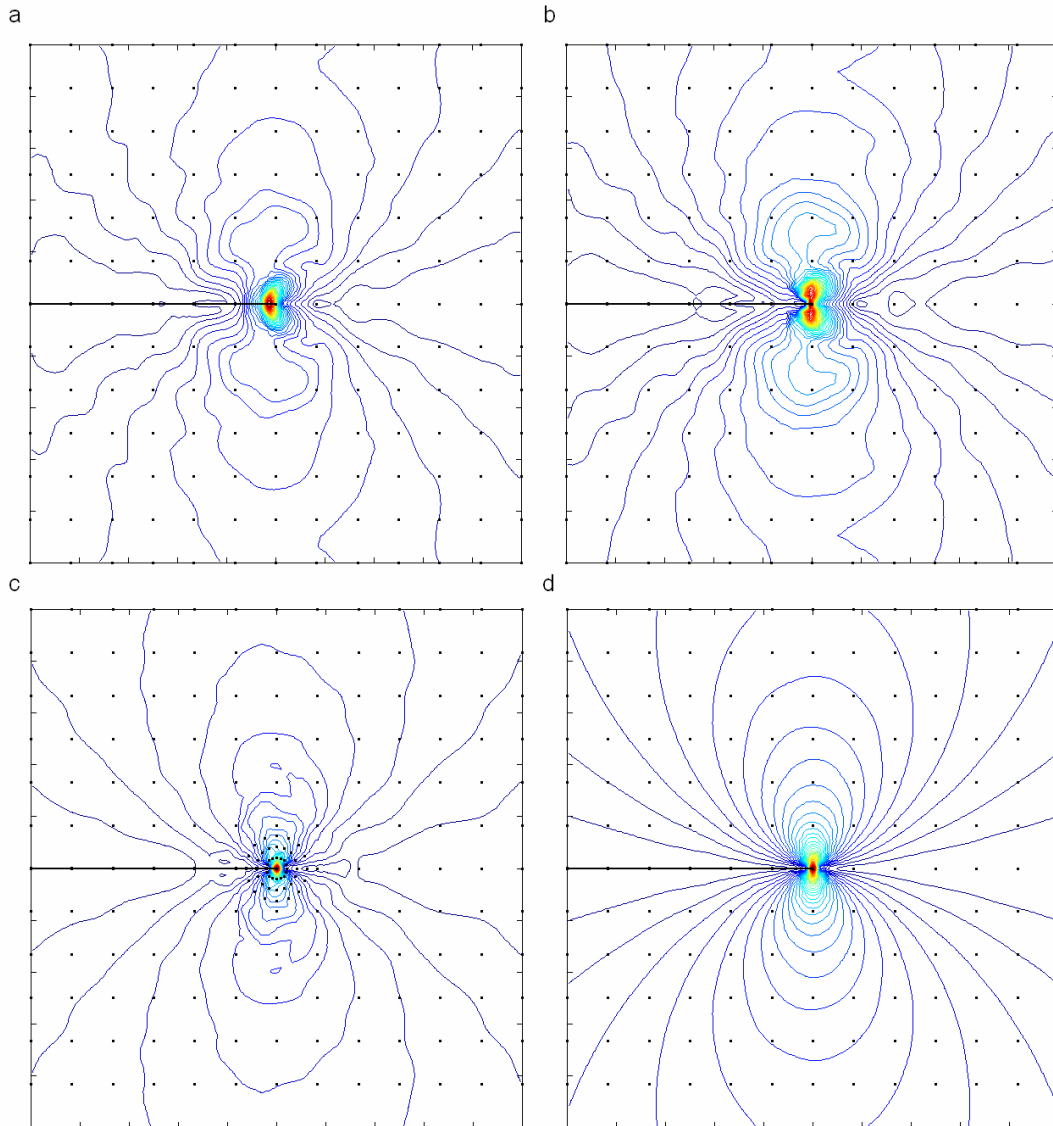


Figure 7. Von Mises stress distribution around crack and nodal distribution:

- a. Diffraction method and linear basis, equally spaced nodal distribution.
- b. Spiral method and linear basis, equally spaced nodal distribution.
- c. Spiral method, basis enrichment, star-shaped array of nodes. *
- d. Spiral method, basis enrichment over entire domain of the problem. *

* Von Mises stress distributions calculated by the diffraction method for cases c. and d. are identical to those calculated by the spiral weight.

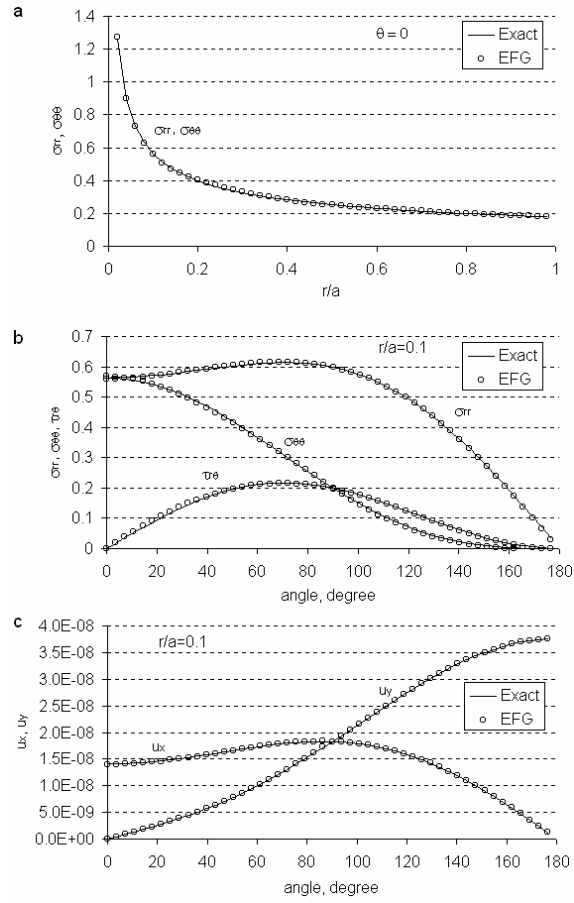


Figure 8. Near-tip of the crack stresses and displacements distributions:

- Radial σ_{rr} and hoop $\sigma_{\theta\theta}$ stresses as a function of distance from the crack tip, r/a for $\theta=0$.
- Angular distribution of radial σ_{rr} , hoop $\sigma_{\theta\theta}$ and shear $\tau_{r\theta}$ stresses for $r = 0.1a$.
- Angular distribution of displacements u_x and u_y , for $r = 0.1a$.

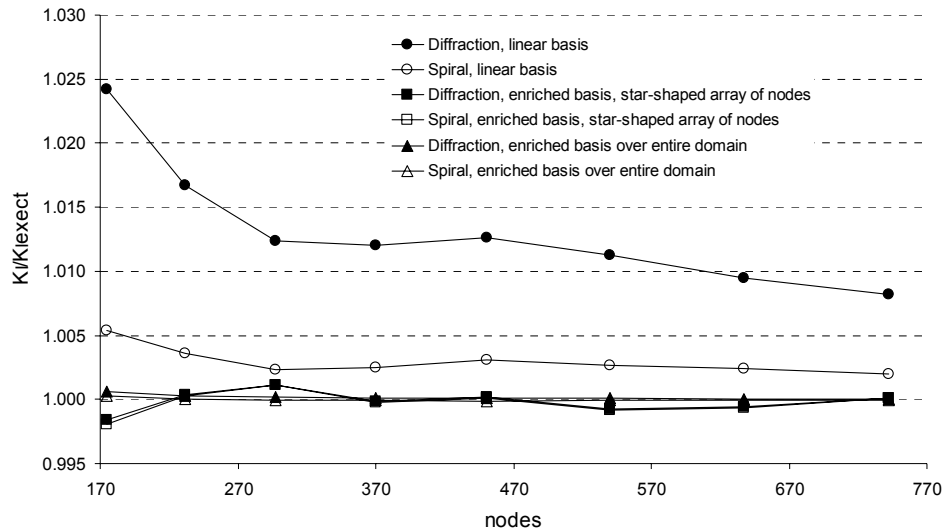


Figure 9. Stress intensity factor as a function of number of nodes in the domain.

Conclusions

A new method, *the spiral weight*, for the construction of weight functions around crack tips is developed to increase the accuracy of EFG approximations for the practically important case of a linear basis. This takes into account the advantages and drawbacks of the diffraction method. The spiral weight functions are constructed to preserve the discontinuity along the entire crack length. A numerical example is solved using different EFG schemes and techniques. The results are calculated, analyzed and compared with the analytical solution, demonstrating the accuracy of the spiral method. It is more accurate than diffraction method in approximations using a linear basis.

References

1. Belytschko, T., Lu, Y.Y., and Gu, L., "Element-Free Galerkin Methods." *International Journal for Numerical Methods in Engineering*, Vol. 37, 1994, pp. 229-256.
2. Belytschko, T., Gu, L., Lu, Y.Y., "Fracture and Crack Growth by Element-Free Galerkin Methods" *Modeling Simulation for Materials Science and Engineering* Vol. 2, 1994, pp. 519-534.
3. Lu, Y.Y., Belytschko, T., Tabbara, M., "Element-Free Galerkin Method for Wave Propagation and Dynamic Fracture" *Computer Methods in Applied Mechanics and Engineering*, Vol. 126, 1995, pp. 131-153.
4. Belytschko, T., Lu, Y.Y., Gu, L., "Crack Propagation by Element-Free Galerkin Methods" *Engineering Fracture Mechanics* Vol. 51(2), 1995, pp. 295-315.
5. Belytschko, T., Lu, Y.Y., Gu, L., Tabbara, M., "Element-Free Galerkin Methods for Static and Dynamic Fracture" *International Journal of Solids and Structures*, Vol. 32(17-18), 1995, pp. 2547-2570.
6. Belytschko, T., Krongauz, Y., Fleming, M., Organ, D., and Liu, W.K., "Smoothing and Accelerated Computations in the Element Free Galerkin Method," *Journal of Computational and Applied Mathematics*, Vol. 74, 1996, pp. 111-126.
7. Belytschko, T., Krongauz, Y., Organ, D., Fleming, M., Krysl, P., "Meshless Methods: An Overview and Recent Developments." *Computer Methods in Applied Mechanics and Engineering*, Vol. 139, 1996, pp. 3-47.
8. Belytschko, T., Tabbara, M., "Dynamic Fracture Using Element-Free Galerkin Methods" *International Journal for Numerical Methods in Engineering*, Vol. 39, 1996, pp. 923-938.
9. Belytschko, T., Krongauz, Y., Fleming, M., Organ, D. J., and Liu, W. K., "Smoothing and Accelerated Computations in the Element Free Galerkin Method." *Journal of Computational and Applied Mathematics*, Vol. 74, 1996, pp. 111-126.
10. Moës, N., Dolbow, J., Belytschko, T., "A Finite Element Method for Crack Growth without Remeshing" *International Journal for Numerical Methods in Engineering* Vol. 46, 1999, pp. 131-150.
11. Muravin, B., Turkel, E., "Advance Diffraction Method as a Tool for Solution of Complex Non-Convex Boundary Problems. Implementation and Practical

- Applications". *Lecture Notes in Computational Science and Engineering: Meshfree Methods for Partial Differential Equations*, (Griebel, M.; Schweitzer, M.A., Eds.) Vol. 26, Springer Verlag, 2002, pp. 307-317.
12. DufLOT, M., "A Meshless Method with Enriched Weight Functions for Three-Dimensional Crack Propagation". *International Journal for Numerical Methods in Engineering* (submitted), 2005.
 13. Rao, B.N., Rahman, S., "An Enriched Meshless Method for Non-Linear Fracture Mechanics." *International Journal for Numerical Methods in Engineering*, Vol. 59, 2004, pp. 197–223.
 14. Belytschko, T., Ventura, G., Xu, J.X., "New Methods for Discontinuity and Crack Modeling in EFG." In *Meshfree Methods for Partial Differential Equations*. (Griebel, M.; Schweitzer, M.A., Eds.), Vol. 26, Springer Verlag, Berlin, 2002.
 15. Krysl, P., Belytschko, T., "Element-Free Galerkin Method: Convergence of the Continuous and Discontinuous Shape Functions." *Computer Methods in Applied Mechanics and Engineering*, Vol. 148, 1997, pp. 257-277.
 16. Terry, T.G., "Fatigue Crack Propagation Modeling Using the Element Free Galerkin Method." *Master's thesis*, 1994, Northwestern University.
 17. Organ, D.J., Fleming, M.A., and Belytschko, T., "Continuous Meshless Approximations for Nonconvex Bodies by Diffraction and Transparency." *Computational Mechanics*, Vol. 18, 1996, pp. 225-235.
 18. Hegen, D., "An Element-Free Galerkin Method for Crack Propagation in Brittle Materials." *Ph.D. thesis*, 1997, Eindhoven University of Technology.
 19. DufLOT, M., Nguyen-Dang, H., "A Meshless Method with Enriched Weight Functions for Fatigue Crack Growth" *International Journal for Numerical Methods in Engineering*, Vol. 59, 2004, pp. 1945-1961.
 20. Irwin, G.R., "Analysis of Stresses and Strains near the End of a Crack Traversing a Plate." *Journal of Applied Mechanics*, Vol. 24, 1957, pp. 361-364.
 21. Williams, M.L., "On the Stress Distribution at the Base of a Stationary Crack." *Journal of Applied Mechanics*, Vol. 24, 1957, pp. 109-114.
 22. Gavete, L., Benito, J.J., Falcon, S., Ruiz, A., "Implementation of Essential Boundary Conditions in a Meshless Method." *Communications in Numerical Methods in Engineering*, Vol. 16, 2000, pp. 409-421.
 23. Fleming, M., Chu, Y.A., Moran, B., Belytschko, T., "Enriched Element-Free Galerkin Methods for Crack Tip Fields." *International Journal for Numerical Methods in Engineering*, Vol. 40, 1997, pp. 1483–1504.
 24. Fleming, M.A., "The Element-Free Galerkin Method for Fatigue and Quasi-static Fracture." *Ph.D. Thesis*, 1997, Northwestern University.